# HYDRODYNAMIC PERFORMANCE OF TWO-DIMENSIONAL UNDULATING FOILS IN TRIANGULAR FORMATION

**M.-H. Chung** *

*Institute of Ocean Engineering and Technology*
*National Kaohsiung Marine University*
*Kaohsiung City, Taiwan 81157, R.O.C.*

## ABSTRACT

As inspired by studies of fish schooling in literature, this work investigates hydrodynamic performance of a two-dimensional undulating-foil triad in viscous flows via numerical simulation. The chord of foil oscillates in the form of a streamwise traveling wave. The triad is in triangular formation, *i.e.*, two foils followed by one. A series of triad configuration are computed assuming the same wave speed, amplitude, and frequency of chord traveling wave for each foil. The results show that, to achieve highest thrust efficiency, the two leading foils should separate from each other by 0.4 chord length, perform anti-phase undulating motion, and the leading edge of the trailing foil stay 0.2 chord length in front of the trailing edges of the leading foils. An underlining mechanism, vortex pair shedding from the leading foil interacting with boundary-layer vorticity field of the trailing foil, has been identified to explain the efficiency enhancement. This optimal triad configuration is different from that obtained in a previous potential flow analysiss.

**Keywords :** Undulating foil, Vortex pair, Efficiency, Numerical simulation.

## 1. INTRODUCTION

Some experimental studies were carried out to study the drag reduction and flow behaviors of the swimming fish [1,2]. In addition, the wakes behind the freely swimming fish or organisms were measured to investigate the high propulsive efficiencies [3-5].

For ordinarily swimming fish, the motion of backbone can be well approximated by a traveling wave [6]. Using this model of backbone motion and assuming inviscid flow, Lighthill [7] and Wu [8] first proposed mathematical theories for flexible elongated bodies and for flat bodies of large aspect ratio, respectively. Along this line, further analytical investigations on hydrodynamics of fish-like propulsion have been extensively performed [9-11].

On the side of numerical simulation, some progress has also been made. Fauci [12] developed a two-dimensional computational model to study the swimming fluid dynamics of flagella and algal cells at Re = 4. Liu *et al.* [13,14] analyzed the hydrodynamics of a tadpole in undulatory motion at Re = 7200 and confirmed that most of the results from the two- and three-dimensional simulations differ little from each other. Carling *et al.* [15] studied self-propelled anguilliform swimming at Re = 3400 by simultaneously solving two-dimensional Navier-Stokes Equations and Newton's laws of motion using finite difference method with coordinate transformation. Shen *et al.* [16] performed a three-dimensional direct simulation to study the turbulent flow at Re = 10200 over a traveling-wavy wall with focus on hydrodynamics related to drag reduction and optimal thrust efficiency. Dong and Lu [17] and Wu *et al.* [18] investigated the hydrodynamics and flow structures around the traveling-wavy body to gain an understanding of fish-like swimming mechanisms.

All the above works deal with a single-fish swimming in undisturbed flows. Some experimental work has been performed to investigate fish swimming in vortex wakes. Liao *et al.* [19,20] and Beal *et al.* [21] found that fish can extract energy from approaching vortices, thereby reducing muscle activity. Liao *et al.* [19] also proposed a model to explain the hydrodynamic advantages implied in this newly found kinematics, the Kármán gait. On the other hand, Gopalkrishnan *et al.* [22] and Streitlien *et al.* [23] experimented on a foil flapping in vortical flows and found that the foil can exploit the energy for efficient propulsion.

Fish school for various reasons, including protection against predator, hydrodynamic exploitation, sociality, and foraging [24,25]. Few theoretical, experimental, and numerical studies have been performed to explore hydrodynamics of fish schooling. Weihs [26,27] first proposed a two-dimensional inviscid flow model to analyze the mechanisms of hydromechanical interaction in fish schools. Under some mathematically convenient assumptions which Partridge and Pitcher [28] questioned

* Assistant Professor, corresponding author


DOI : 10.1017/jmech.2011.21
Copyright © 2011 The Society of Theoretical and Applied Mechanics, R.O.C.
https://doi.org/10.1017/jmech.2011.21 Published online by Cambridge University Press

later for real schools, his arguments justify the "diamond" pattern actually found in some sorts of fish [29]. Deng *et al*. [30] has numerically studied propulsive performance of two fish-like swimming foils in tandem and concluded that the trailing individual can acquire higher thrust than that generated by a single swimming fish. Recently, Dong and Lu [31] performed simulation of flow over traveling-wavy foils in a side-by-side arrangement. They investigated the effects of lateral spacing and phase difference between adjacent foils and identified some vortex structures in the wake. For a simple array of three flapping rigid foils (one leading two), Kelly and Xiong [32] experimentally studied the effects of geometric and kinematic parameters and proposed a potential flow model to qualitatively explain the vortex wake-body interactions in schooling aquatic locomotion. Later, Eldredge *et al*. [33] performed corresponding viscous computations. Note all the above theoretical and numerical studies fall under the two-dimensional category.

For real fish schools, Breder [34] identified a single type of space lattice to approximate the arrangement of fishes in a school based on geometrical reasoning and supported by empirical data. He attributed the structure and maintenance of fish schools to the interaction of space lattice, vortex trails, and the lubricity of fish surface mucus. When the fishes are deployed according to the "fish school" lattice, which is close to Weihs's diamond pattern, the lubricity of the mucus- water mixture left by the fish ahead in its vortices decreases the drag on the following fish. In contrast with the diamond pattern, Partridge and Pitcher [28] had observed three species of schooling fish and found that the trailing fish snout is often located in front of the tails of the leading fish, fish had no tendency to position themselves centrally between pairs of leading fish, and neighbouring fish have no consistent phase relationship. Therefore, fish could not have benefited from induced velocity from vortex trails of leading fish.

As demonstrated above, Breder's model and observation of Partridge and Pitcher differ distinctly in the school pattern. Many aspects need to be clarified before underlying mechanisms can be identified. In the hydrodynamic aspect, clarification of possible mechanisms is relevant only in three-dimensional configurations due to highly three-dimensional fish-body geometries and fluid flows. Therefore neither the present two-dimensional numerical simulation nor the Weihs's calculation [27] can draw any meaningful conclusion on mechanisms to form real fish school patterns. However, regarding the two-dimensional foil triad as a novel thrust generator, the present work would give more reliable results than the Weihs's model.

Based on Weihs's potential flow analysis [26], the diamond pattern has the hydrodynamic advantage that the trailing individual can exploit the combined effect of reverse Kármán vortex streets shed by the two leading individuals. This inspired the current work. We consider three undulating foils in triangular formation, two foils leading one, which constitute the major part of the "diamond" pattern. The propulsive performance of this foil triad is investigated under the notion of Froude efficiency, that is, given an incoming flow velocity, both thrust and efficiency will be evaluated via two-dimensional numerical simulation. The purposes of this work include (1) to find the most efficient configuration of the triangular formation and (2) by a series of viscous computations to reexamine the hydrodynamic advantages of the "diamond" pattern derived from the inviscid analysis. Notably, as a novel thrust generator, the foil triad is an inspiration from fish schooling but we can not predict the hydrodynamics of real three-dimensional fish schooling using the present results of two-dimensional study.

## 2. MATHEMATICAL FORMULATION AND NUMERICAL METHOD

### 2.1 Governing Equations

Flow over undulating foils in triangular formation is considered in this work (Fig. 1). The two-dimensional incompressible Navier-Stokes equations are employed as governing equations for fluid flow. To nondimensionalize the equations, the chord length of foil, $L$, is used as the length scale, and the free-stream velocity $U$ as the velocity scale. The integral nondimensional equations are then given as

$$\oint_{cs} \mathbf{u}\cdot\mathbf{n}\,dS = 0\,, \tag{1}$$

$$\frac{\partial}{\partial t}\int_{cv}\mathbf{u}dV + \oint_{cs}\mathbf{u}(\mathbf{u}\cdot\mathbf{n})\,dS = -\oint_{cs} p\,\mathbf{n}\,dS + \frac{1}{\mathrm{Re}}\oint_{cs}\nabla\mathbf{u}\cdot\mathbf{n}\,dS\,, \tag{2}$$

where $\mathbf{u}$ represents the fluid velocity vector, $p$ the pressure normalized by $\rho U^2$ with $\rho$ the fluid density, and Re is the Reynolds number defined as $\mathrm{Re} = UL/\nu$ with $\nu$ the kinematic viscosity. *cv* and *cs* denote the control volume and control surface, respectively, and $\mathbf{n}$ is the outward unit vector normal to the control surface.

NACA0012 airfoil shape is used as the contour of foil at an equilibrium position of undulating motion. The chord is making a nearly lateral oscillation in the form of a wave traveling in the streamwise direction, described by

$$y^i(x,\,t) = A(x)\cdot\sin\left[2\pi(x-h^i-ct)+\phi_i\right]+d^i\,,$$
$$h^i \le x \le h^i + X_{\mathrm{END}}\,, \tag{3}$$

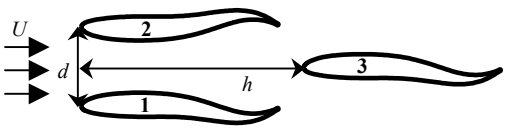



Fig. 1 Schematic of the flow configuration: Undulating foils in triangular formation



https://doi.org/10.1017/jmech.2011.21 Published online by Cambridge University Press

where the superscript "$i$" represents the $i$th foil, $A$ is the amplitude, $c$ the phase speed, $\phi_i$ the phase angle, $h^i$ the streamwise position of the leading edge, $d^i$ the lateral position of the chord line in the equilibrium condition, and $X_{\mathrm{END}}$ the length measured from leading to trailing edge along $x$-axis. The phase speed and amplitude are assumed the same for each foil. For the triangular formation of Fig. 1,

$$h^1 = 0\ , \quad h^2 = 0\ , \quad h^3 = h\ ,$$
$$d^1 = -d/2\ , \quad d^2 = d/2\ , \quad d^3 = 0\ . \tag{4}$$

To mimic the backbone undulation of fish swimming, the amplitude $A(x)$ is approximated by a quadratic polynomial of which the coefficients are solved from the kinematic data of a steadily swimming saithe. We assume that both the thickness distribution along the chord and the chord length keep unchanged during the course of undulation. The latter assumption determines $X_{\mathrm{END}}$. Refer to [35] for details in determining $A(x)$ and $X_{\mathrm{END}}$.

Throughout the calculations in this work, the computational domain is a square region, $[-10,22] \times [-16,16]$, with a free-slip condition at the bottom and the top boundaries. Unit velocity is prescribed at the left (inflow) and right (outflow) boundaries. On the surfaces of the traveling-wavy foils, no-slip condition is used.

### 2.2 Simulation Parameters

The Reynolds number is set as 5000 in this study, a value relevant to the motion of an aquatic animal at intermediate Reynolds numbers. Without loss of generality, $\phi_1 = 0°$ is fixed through all computations of this work. The parameters studied include lateral spacing between upstream foils, $d$, streamwise spacing between the first and second row, $h$, phase difference of the second leading foil relative to the first one, $\phi_2$, and phase difference of the trailing foil relative to the first leading foil, $\phi_3$. Specifically, nine streamwise spacings are examined, *i.e.*, $h$ = 0.6, 0.7, 0.8, 0.9, 1, 1.1, 1.2, 1.6, and 2, for each of four lateral spacings, $d$ = 0.4, 0.5, 0.6, and 0.8, with a pair of phase differences, $(\phi_2, \phi_3) = (180°, 0°)$. To investigate the effect of $\phi_2$ and $\phi_3$, we simulated the cases with $d = 0.4$ and various combinations of $(\phi_2, \phi_3)$ at intervals of 90° for $h$ = 0.6, 0.8, 0.9, 1, 1.1, and 1.2. Meanwhile, this study simulated dual-foil formations with different $\phi_2$ to clarify the role of the trailing foil in the triangular formation.

### 2.3 Performance Parameters

Thrust and efficiency of a thrust generator are two important parameters quantifying and analyzing the propulsive performance and the associated flow fields. In the present approach to propulsive performance, a free stream with constant velocity is flowing over the foil triad which is fixed with respective to the inertial reference frame. Therefore the thrust coefficient is defined as

$$C_T = 2F_T/(\rho U^2 L)\ , \tag{5}$$

where $F_T$ is the net thrust force defined by

$$F_T = \oint_{\textit{foil surface}} \left[ (f^p \mathbf{n} + f^v \mathbf{s}) \cdot \mathbf{i} \right] dA \tag{6}$$

where $f^p$ and $f^v$ are the pressure and the viscous force exerted on ambient fluid per unit area of the foil surface, $\mathbf{n}$ the outward unit normal vector, $\mathbf{s}$ the tangential unit vector, and $\mathbf{i}$ the unit vector in the $x$ direction.

The thrust efficiency is defined as the ratio of the useful power to the mechanical power input in a time-average sense (Froude efficiency):

$$\eta = \frac{\langle F_T \rangle U}{\langle P \rangle} = \frac{\langle C_T \rangle}{\langle C_P \rangle}\ , \tag{7}$$

where $< \cdot >$ denotes the averaging operator over one period of foil undulation and the power coefficient $C_P$ is defined by

$$C_P = 2P/(\rho U^3 L) \tag{8}$$

with $P$ the instantaneous mechanical power input to the ambient fluid by the foil undulation,

$$P = \oint_{\textit{foil surface}} \left[ (f^p \mathbf{n} + f^v \mathbf{s}) \cdot \mathbf{u}_b \right] dA\ , \tag{9}$$

$\mathbf{u}_b$ being the local foil-surface velocity.

### 2.4 Numerical Method

This study solves all of the governing equations by the cell-centered collocated finite-volume pressure-free projection method with the cut-cell Cartesian-grid approach to immersed arbitrarily moving bodies [36,37]. The present Reynolds number, 5000, could cause turbulent flows near or behind the foil. To justify the assumption of laminar flow in this study, we performed some simulations for a NACA0012 foil pitching about one-quarter-chord position with pitching amplitude of 2° at Re = $1.2 \times 10^4$. The grid density near the foil surface is the same as that used in this study. Figure 2 compares the results with those in the experimental work of Bohl and Koochesfahani [38] in terms of the mean thrust coefficient $< C_T >$ versus reduced frequency $k \equiv \pi f L / U$, where $f$ is the pitching frequency. The three reduced frequencies currently selected, $k$ = 5.7, 9, and 11.5, correspond to negative, nearly zero, and positive mean thrust respectively. The agreement is pretty good for each selected reduced frequency. Finally, because the decay of velocity deficit in the wake follows a similar rule for both laminar and turbulent flows over a flat plate, we can argue that the conclusion about the hydrodynamics of the trailing foil in this study would not be significantly affected if this foil confronts turbulent wake flows from the leading foils. In brief, the laminar-flow computations are reasonable for this study if we note that the current Reynolds number is below half of that in the above case of justification.



https://doi.org/10.1017/jmech.2011.21 Published online by Cambridge University Press

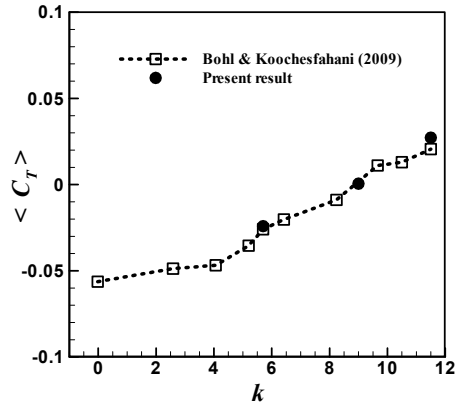



Fig. 2 Mean thrust coefficient $<C_T>$ versus reduced frequency $k$ for a NACA0012 foil pitching about one-quarter-chord position with pitching amplitude of 2° at Re = $1.2 \times 10^4$. Comparison between the experimental results of Bohl and Koochesfahani [38] and the present calculations

## 3. RESULTS AND DISCUSSION

This section presents some simulation results for the flow characteristics of foil-triad propulsion. Computational results of single-foil and foil-duad propulsion are also included for comparison. Some hydrodynamic quantities, including the net thrust force, the power consumption, and the thrust efficiency, are analyzed. Moreover, the vortex structures in the wake of foils in selected configurations of triangular formation are exhibited and studied. Because a flow state exhibiting periodic variation of time-dependent forces and powers can be reached after 3 ~ 4 cycles for all cases considered, the periodic-mean values are obtained by time-averaging over the fifth and sixth cycles.

### 3.1 Single-Foil Propulsion

In the previous work [35], we have simulated single-foil propulsion and verified the results against the predictions of Dong and Lu [31]. Therefore, a minimum mesh size of 1/256 is used in this work to assure grid-independent results.

### 3.2 Foil-Triad Propulsion

According to the previous computational results [31] for a single-foil propulsion, the periodic-mean net thrust force is nearly zero at $c = 1.5$ and positive at $c = 2$; the latter is selected as the phase speed fixed throughout this work. The effect of aforementioned simulation parameters on propulsive performance is the primary concern.

#### 3.2.1 Effect of Lateral and Streamwise Spacings

For a two-dimensional fish school whose elementary unit is a fish triad similar to Fig. 1, Weihs's calculation [27] indicated that, the trailing fish can acquire the most of the energy of thrust vortices shed by the two leading fish which are separated by 0.4 body length and beat their tails in anti-phase. Meanwhile, the trailing fish should stay five tail beats behind the tail tips of the leading fish. Thus we chose $\phi_2 = 180°$ and $\phi_3 = 0°$ to analyze the effects of lateral spacing, $d$, and streamwise spacing, $h$. Figure 3 shows the periodic-mean thrust coefficient, periodic-mean power coefficient, which are both averaged over three foils, and the thrust efficiency as function of $h$ at various $d$ for the foil triad as a whole. Based on the efficiency plot, the foil-triad is always more efficient than the single-foil propulsion for the considered phase differences. For each lateral spacing, efficiency varies little between $h = 1.2$ and 2 and rises as $h$ decreases from 1.2 to 0.8 at a rising rate which is faster for smaller lateral spacing. Further decreasing $h$ causes rapid efficiency loss. At the predicted best position for the trailing foil, $h = 0.8$, efficiency increases as lateral spacing decreases.

By Eq. (7), the thrust efficiency is the periodic-mean thrust coefficient divided by periodic-mean power coefficient. Therefore we can explain the variation of efficiency by analyzing the variation of these two coefficients. From the thrust and power plots (Fig. 3), the tendency of thrust variation is very similar to that of efficiency, demonstrating that thrust variation dominates power variation as a source of efficiency variation. The relative scales of the variations in the thrust coefficient and in the power coefficient can be measured by $(<C_T>_{max} - <C_T>_{min}) / (<C_T>_{max} + <C_T>_{min})$ and $(<C_P>_{max} - <C_P>_{min}) / (<C_P>_{max} + <C_P>_{min})$ respectively. Their values are approximately 1/3 and 1/5, which quantitatively confirm the dominance of thrust over power.

To dig into the role of each foil in the triad, Fig. 4 shows the periodic-mean thrust coefficient as function of streamwise spacing at various lateral spacings for each foil. The two leading foils exhibit similar trend, an expected result consistent with the anti-phase configuration, and almost the same value for $h > 1.6$, suggesting the influence of the trailing foil is negligible for streamwise spacings greater than 1.6 chord length. This phenomenon is reasonable because the leading foil can only feel the trailing foil by potential flow effect, which is inversely proportional to the distance squared. Furthermore, for sufficiently close lateral spacings ($d = 0.4$ and 0.5), the leading foils always generate a larger thrust than the single-foil propulsion, regardless of the position of the trailing foil. When the leading edge of the trailing foil is located upstream of the trailing edge of the leading foil, the net thrust force of the leading foil increases rapidly as $h$ decreases and hits the maximum at $h = 0.8$ and 0.9 for $d = 0.4$ and 0.5, respectively. For the trailing foil, the net thrust force remains nearly constant (very close to that of the single-foil propulsion) when $h > 1.2$ and increases with decreasing $h$ when $h < 1.2$ for $d = 0.8$. However, a depression region exists for other lateral spacings; the most obvious occurs for $d = 0.4$ (the maximum net thrust force at $h = 0.6$ is 400% the minimum at $h = 1$). Note that the trailing-foil thrust is still dependent on $d$ for the largest streamwise spacing ($h = 2$) because the trailing foil feels the leading foils both by viscous-wake effect and potential-flow effect, of which the former travels farther than the latter.



https://doi.org/10.1017/jmech.2011.21 Published online by Cambridge University Press

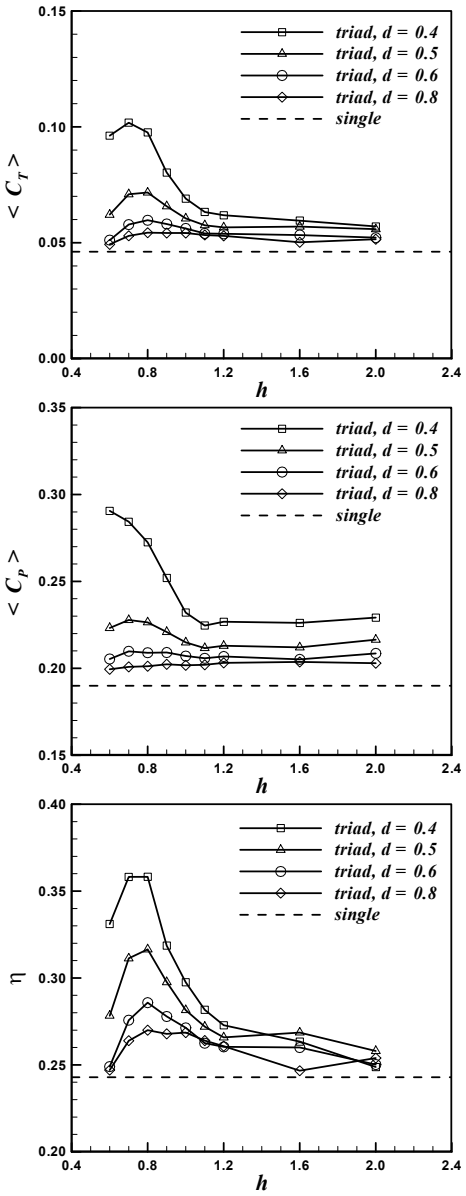



Fig. 3 Periodic-mean thrust coefficient, periodic-mean power coefficient, and thrust efficiency as function of streamwise spacing, $h$, at various lateral spacings, $d$. Both coefficients are averaged over three foils and efficiency is evaluated for the triad as a whole ($\phi_2 = 180°$ and $\phi_3 = 0°$). Dashed line indicates the corresponding value for the single-foil propulsion

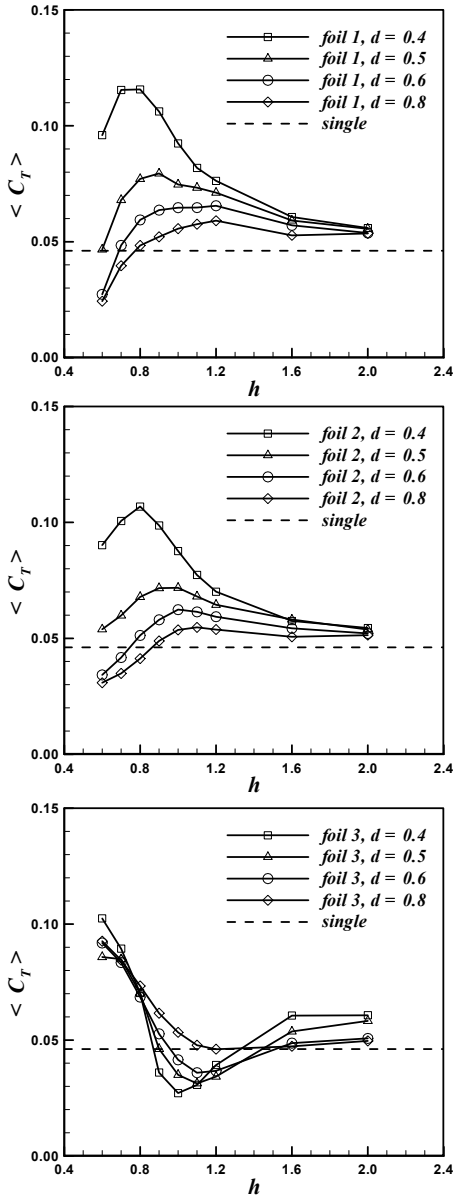



Fig. 4 Periodic-mean thrust coefficient as function of streamwise spacing at various lateral spacings for each foil in the foil triad with $\phi_2 = 180°$ and $\phi_3 = 0°$. Dashed line indicates the value for the single-foil propulsion

Figure 5 shows the periodic-mean power coefficient as function of streamwise spacing at various lateral spacings for each individual foil. Again, a similar trend exists for both the leading foils with almost the same level at $h = 2$. For the trailing foil, the power coefficient varies less than the leading foils do, especially for $d = 0.4$ and $h < 1$.

With the thrust and power coefficients obtained, the thrust efficiency of each foil can be calculated (Fig. 6). For the widest lateral spacing ($d = 0.8$), the leading-foil efficiency cannot be raised significantly as the trailing foil joins the leading-foil duad. The trailing-foil efficiency remains the single-foil-propulsion level when the streamwise spacing is large ($h > 1.2$) but increases steeply as $h$ decreases for a small $h$. As the lateral spacing decreases further, the leading foils benefit more from joining the trailing foil, at least for $h = 2$ to 0.8. Particularly at $d = 0.4$ and $h = 0.8$, the efficiency of Foil 1 is approximately 58% higher than the single-foil-propulsion level. At these smaller lateral spacings, the efficiency of the trailing foil will be enhanced mildly when staying at a large streamwise spacing ($h > 1.6$) and reduced gradually below the single-foil-propulsion level from $h = 1.6$ to $h = 1.2 \sim 1$. For even smaller $h$, the trailing-foil efficiency rises very rapidly, reaching a maximum of approximately 2.1 times the single-foil-propulsion level at $h = 0.6$.



https://doi.org/10.1017/jmech.2011.21 Published online by Cambridge University Press

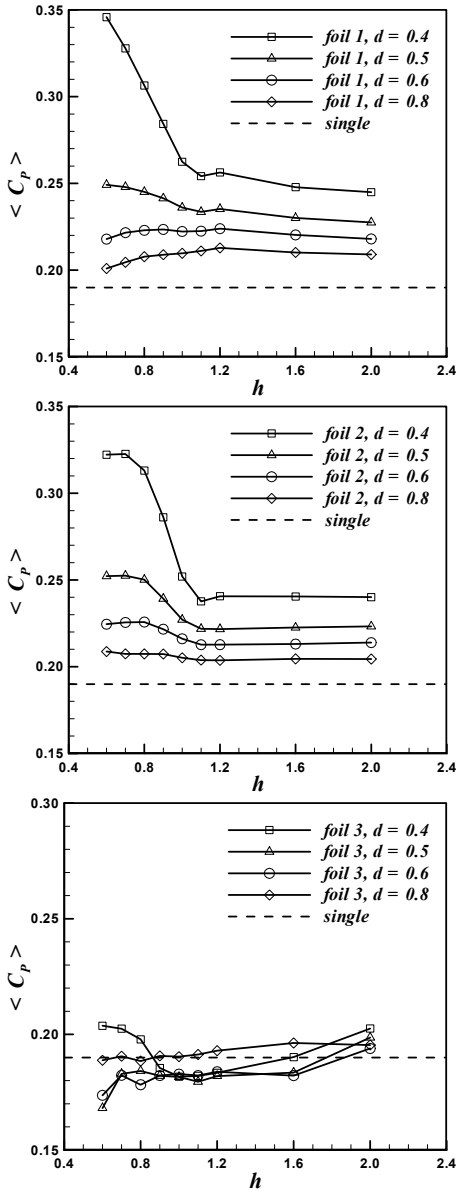



Fig. 5 Periodic-mean power coefficient as function of streamwise spacing at various lateral spacings for each foil in the foil triad with $\phi_2 = 180°$ and $\phi_3 = 0°$. Dashed line indicates the value for the single-foil propulsion

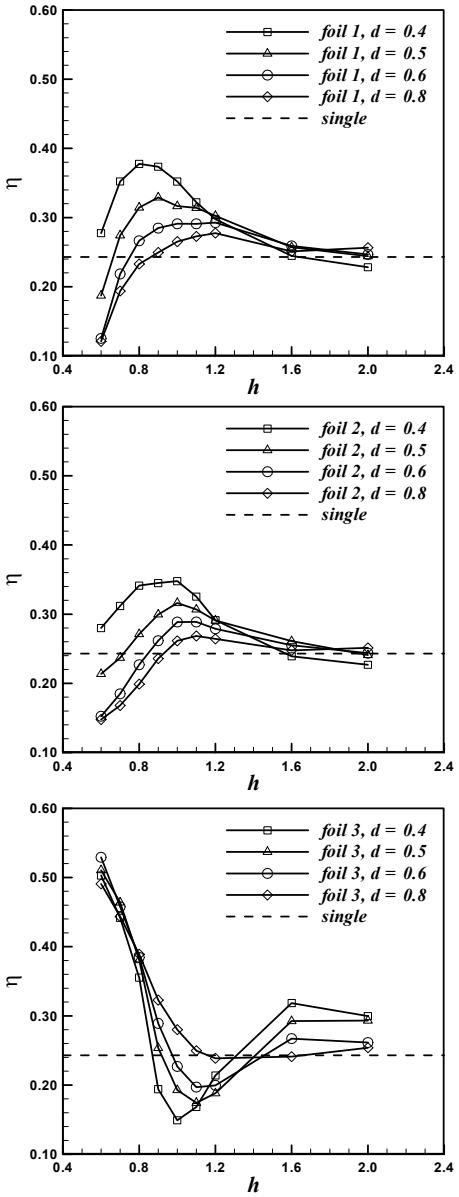



Fig. 6 Thrust efficiency as function of streamwise spacing at various lateral spacings for each foil in the foil triad with $\phi_2 = 180°$ and $\phi_3 = 0°$. Dashed line indicates the value for the single-foil propulsion

At $d = 0.4$, the efficiency of the trailing foil reaches the maximum value of 0.5 at $h = 0.6$ and the minimum value of 0.15 at $h = 1$. However, the efficiency of the leading foils shows minor difference (< 0.08) between these two streamwise spacings. Therefore, the contrast between the two cases of $h = 0.6$ and $h = 1$ should be able to clarify the mechanism of efficiency enhancement of the trailing foil.

Figure 7 presents the time-dependent thrust and power coefficients during the sixth period of undulation for each foil in the two cases. For $h = 0.6$ (Fig. 7(a)), the generated net thrust force of the leading foils deviates little from that of the single-foil-propulsion level through the course of undulations except times near $t/T = 5/8$. The net thrust force generated by the trailing foil generally always differs from the single-foil-propulsion level with the maximum occurring near $t/T = 5/8$. The periodic-mean thrust coefficient for each of the three foils are roughly the same as shown in Fig. 7(a). Conversely, the power consumed by the leading foils is larger than the single-foil-propulsion level through the course of undulation and peaks near $t/T = 5/8$. The trailing foil consumes power at nearly the single-foil-propulsion level. The periodic-mean power coefficients for the leading foils become considerably greater than that for the trailing foil (Fig. 5). Eventually, the trailing foil has much better efficiency than the leading foils (Fig. 6); however, both above the single-foil-propulsion level. For $h = 1$ (Fig. 7(b)), the leading foils have approximately the same thrust generation as the trailing foil during $t/T = 3/8 \sim 7/8$ and is higher for the remaining period. Additionally, the



https://doi.org/10.1017/jmech.2011.21 Published online by Cambridge University Press

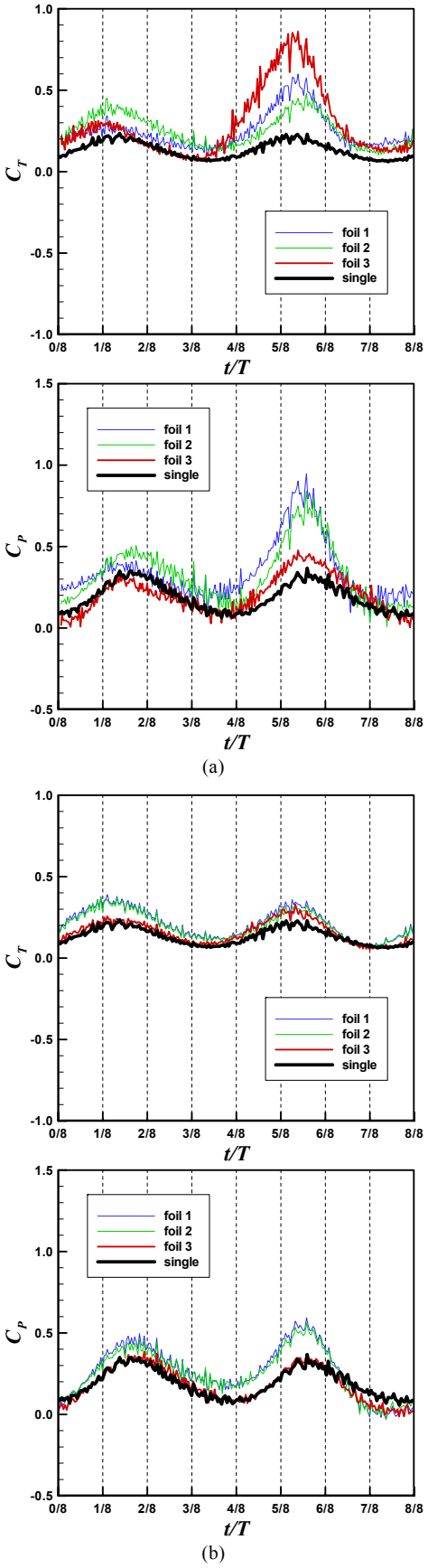



Fig. 7 Time-dependent thrust and power coefficients during the sixth period of undulation for each foil in the foil triad with $\phi_2 = 180°$, $\phi_3 = 0°$, $d = 0.4$ and (a) $h = 0.6$ (b) $h = 1$, compared with that of the single-foil propulsion

leading foils consume slightly more power than the trailing foil throughout the whole period. The efficiency obtained is higher and lower than that of the single-foil-propulsion level for the leading and trailing foils, respectively. The combined effect generates a higher foil-triad efficiency for $h = 0.6$ than that for $h = 1$ by 0.035 (Fig. 3).

Figure 8 presents the pressure contours at $t/T = 5/8$ for $h = 0.6$ and $h = 1$, both at $d = 0.4$. For $h = 0.6$, a low-pressure region ($x = 0.6 \sim 1$) exists around the anterior part of the trailing foil. This low pressure is caused by a high-speed flow in the lateral gap between the leading foils and the trailing foil. The flow velocity increases after entering the small-area gap region because mass flow rate must be conserved. This mechanism is also called the Venturi effect. For $h = 1$, however, pressure in the lateral gap between the two leading foils is minimal at $x \approx 0.7$, increases rapidly downstream, and does not cause low pressure near the head of the trailing foil. Because the pressure force, compared with the viscous force, is the major part of the net thrust force at the Reynolds number studied, the significant difference between the two streamwise spacings in the pressure field around the head of the trailing foil generates a larger net thrust force for $h = 0.6$ than for $h = 1$.

Considerable insight can be gained when the distribution of the upstream directed component of the hydrodynamic force per unit area applied to the foil surface at this particular time is depicted appropriately. Figure 9 provides this information for the two streamwise spacings. Clearly, the distribution of force per unit area on the trailing foil surface is distinctly different between the two streamwise spacings. For $h = 0.6$, the large positive component on the anterior surface of the trailing foil is consistent with the existence of the low-pressure region already mentioned. This depression of pressure originates in reaction to the movement of the coherent vortex pair with a small jet angle, as further explained later. For the leading foils, the net thrust force of each foil for $h = 0.6$ is slightly higher than that of the corresponding individual foil for $h = 1$, with difference between two Foil 1 more than that between two Foil 2. Figure 10 depicts the distribution of power consumption per unit area on the foil surface at this particular time. The distribution of power consumption per unit area on the trailing foil surface is slightly different between the two streamwise spacings. However, on the posterior gap-facing side of each leading foil, the power consumption per unit area for $h = 0.6$ is nearly double that for $h = 1$. This analytical finding is not surprising because this portion of the foil surface is only moving to widen the aforementioned low-pressure region at this instant. In short, for the trailing foil, the streamwise spacing significantly affects the net thrust generation but only slightly affects the power consumption. For the leading foils, the effect of the streamwise spacing is mild on the net thrust generation and slightly stronger on power consumption.



https://doi.org/10.1017/jmech.2011.21 Published online by Cambridge University Press

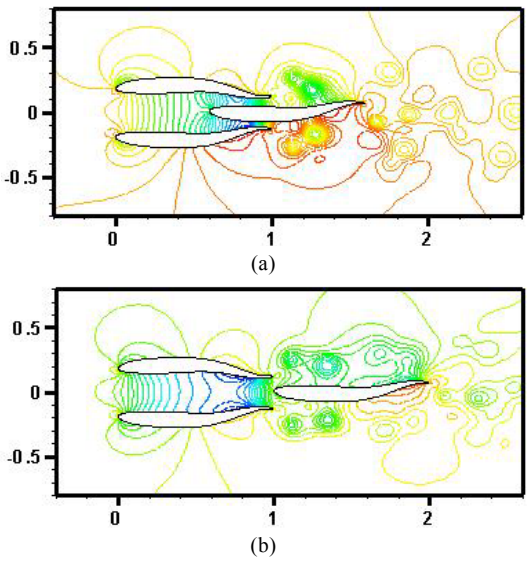



Fig. 8 Pressure contour at $t/T$ = 5/8 during the sixth period of undulation for the foil triad with $\phi_2$ = 180°, $\phi_3$ = 0°, $d$ = 0.4 and (a) $h$ = 0.6 (b) $h$ = 1

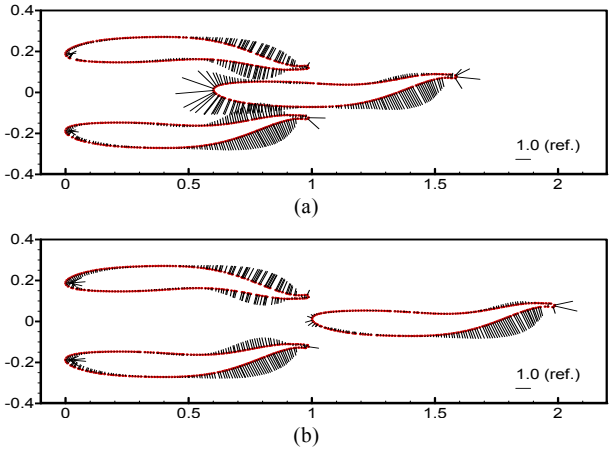



Fig. 9 Distribution of upstream directed component of hydrodynamic force per unit area applied to the foil surface in the foil triad at $t/T$ = 5/8 with $\phi_2$ = 180°, $\phi_3$ = 0°, $d$ = 0.4 and (a) $h$ = 0.6 (b) $h$ = 1. The length of solid lines perpendicular to foil surfaces represent the local magnitude of force per unit area. Positive and negative contributions are indicated by the direction pointing outward and inward, respectively. Dimensionless free-stream pressure is 1

The relative motion between the leading foils and the trailing one generates a pressure field around the trailing foil which differs from that of the single-foil propulsion only near the anterior part of the trailing foil. Note that the posterior part of foil, which has larger undulating amplitude than the anterior part, takes charge of most power generation. Eventually, the above relative motion hardly changes the time history of the power coefficient for the streamwise spacing equal to either 1 or even 0.6, as clearly shown in Figs. 7(a) and 7(b). On the other hand, for $h$ = 1, the streamwise hydrodynamic force integrated over the anterior part of the trailing foil is almost the same as

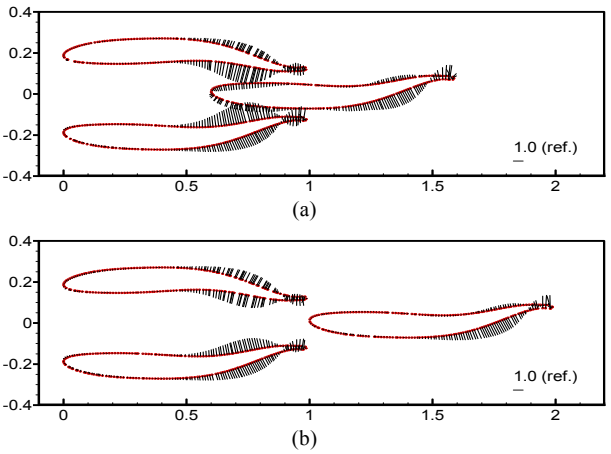



Fig. 10 Distribution of power consumption per unit area on the foil surface in the foil triad at $t/T$ = 5/8 with $\phi_2$ = 180°, $\phi_3$ = 0°, $d$ = 0.4 and (a) $h$ = 0.6 (b) $h$ = 1. The length of solid lines perpendicular to foil surfaces represent the local magnitude of power consumption per unit area. Positive and negative contributions are indicated by the direction pointing outward and inward, respectively. Dimensionless free-stream pressure is 1

that of the single-foil propulsion. However, for $h$ = 0.6, the value of this force is sensitive to the leading-foil motions. In particular, when the aforementioned Venturi effect is strongest ($t/T \approx$ 5/8), the algebraic magnitude of this force is significantly less than that of the single-foil propulsion. In brief, for the trailing foil, the power consumption almost remains unchanged but the thrust force (negative streamwise hydrodynamic force integrated over the whole foil surface) increases obviously when $h$ decreases from 1 to 0.6. Refer to the foil-3 curve with $d$ = 0.4 in Figs. 4 and 5. Therefore the individual efficiency of the trailing foil is enhanced significantly for this change of $h$. Refer to the foil-3 curve with $d$ = 0.4 in Fig. 6.

The relative motion between the leading and trailing foils generates a pressure field around the leading foils which differs from that of the foil-duad propulsion near the posterior parts of the leading foils. Therefore both of the power consumption and the thrust force would be different from that of the foil-duad propulsion. Around $t/T$ = 5/8, the strong Venturi effect associated with $h$ = 0.6 greatly lowers the pressure between the posterior parts of the leading foils, with respect to the situation in $h$ = 1. Because the posterior parts of the leading foils are deflected toward each other around this instant, the pressure difference between the two sides of the posterior part of each leading foil is in favor of the thrust force. However, the posterior parts of the two leading foils are moving away from each other around this instant. Noting that the pressure between the two posterior parts is lower than the outside pressure, the power consumption turns to be higher than that of $h$ = 1, also. Scrutinizing the curves for foil 1 and foil 2 in Fig. 7, we find that the relative increment of the thrust coefficient is approximately the same as that of the



https://doi.org/10.1017/jmech.2011.21 Published online by Cambridge University Press

power coefficient around this instant. In other words, the individual efficiency of the leading foil can not be enhanced significantly for this change of $h$. In fact, it is decreased when $h$ changes from 1 to 0.6. Refer to the foil-1 or foil-2 curve with $d = 0.4$ in Fig. 6.

In summary, the optimal efficiency is reached through the interaction between the leading and trailing foils. The essence of this interaction comes from the undulatory kinematics of carangiform swimmers, that is, amplitude is large over the posterior part but small over the anterior part of the foil.

The above-mentioned Venturi effect explains the difference of performance between $h = 0.6$ and $h = 1$ near $t/T = 5/8$. Further explanations can be made and insight gained by studying transient vortex structures. Figure 11 presents series of the vorticity contour snapshots in the sixth period of undulation for the foil triad with $h = 0.6$ and $h = 1$. A reverse Kármán vortex street is clearly shed from the tail tips of the leading foils for both streamwise spacings. Note the vortex pairs for $h = 0.6$ exhibit more compact structures than those for $h = 1$. However, the jet angle of vortex pair, $\alpha$, which is defined as the angle between the streamwise direction and the jet flow separating the two opposite-sign vortices, is smaller for shorter streamwise spacing. To explore the mechanism of vortex shedding from either leading foil, attention is focused on a specific vortex pair shedding from the upper foil (Foil 1). That is, a negative vortex (minus sign in white) is just shedding and a positive vortex (plus sign in white) is to be shed from Foil 1 for either streamwise spacing at $t/T = 0/8$ and $t/T = 5/8$ respectively. During this period of time, the downstream-moving negative vortex in the case of $h = 0.6$ is strongly interacted with, or "dragged by", the mainly negative vorticity field of the boundary layer flow over the upper surface of the trailing foil. This interaction retards the motion of the shedding negative vortex in both the downstream and transverse directions. For $h = 1$, this "dragging" effect is not obvious because the relevant boundary-layer vorticity field of the trailing foil is distant from the shedding negative vortex. Eventually, the two opposite-sign vortices come closer to each other and form a smaller jet angle for $h = 0.6$ than for $h = 1$.

Considering two-dimensional vortex pairs as cross-sectional structures of three-dimensional vortex rings, the momentum $I$ of a single small-core vortex ring can be derived according to Milne-Thomson [39]:

$$I = \rho \Gamma \pi R^2 , \qquad (10)$$

where $\Gamma$ is the circulation about a curve enclosing the vortex ring and $R$ the radius of the vortex ring. Because the vortex ring is formed during almost the same time for both streamwise spacings, this momentum, multiplied by $\cos \alpha$, can be regarded as the thrust force provided by the vortex ring. Table 1 presents the kinematics of the vortex pair at $t/T = 5/8$ as representative, if $R$ and $\alpha$ are calculated from the positions where the maximal positive vorticity ($\omega_+$) and the minimal negative vorticity ($\omega_-$) occur. Assuming that $\Gamma \propto (\omega_+ - \omega_-)$, the vortex-pair momentum for $h = 0.6$ is 0.522 times that for $h = 1$. However, the vortex-pair thrust force for $h = 0.6$ is 1.612 times that for $h = 1$. That is, in contrast to $h = 1$, the larger thrust force for $h = 0.6$ comes from the jet generated by the vortex pair whose axis is more inclined to the streamwise direction though momentum is weaker. At this instant, this jet flow is a manifestation of the above-mentioned Venturi flow, and vice versa.

Situation is very similar for the vortex pairs shed from the lower leading foil (Foil 2). The difference between the two streamwise spacings in the vortex structures behind the trailing foil is considered minor because anterior disturbances are little felt by the posterior part of the foil, as has been illustrated in Figs. 9 and 10. By the way, a vortex-pair can be subjectively regarded as being generated by a specific foil, but the contribution to thrust force is shared by all foils involved. In summary, the efficiency enhancement of the foil triad for $h = 0.6$ is achieved by leading-foil-shed vortices interacting with the boundary-layer vortices on the trailing-foil surface. This interaction produces a sufficiently small vortex-pair jet angle that the thrust-force increment can compensate for the increase of power consumption, that is, efficiency is raised.

### 3.2.2 Effect of Phase Difference

Due to the higher efficiency for $d = 0.4$ than for other lateral spacings, the effect of varying $\phi_2$ and $\phi_3$ on the efficiency is examined at this lateral spacing for selected streamwise spacings. Figure 12 collects some key results. First, the efficiency decreases with increasing $h$ as $h \geq 0.8$ for each combination of $\phi_2$ and $\phi_3$, not only for the (180° and 0°) pair. Second, comparison of the efficiency between the duad and the triad for the same $\phi_2$ reveals that adding a trailing foil to a foil duad can enhance the efficiency of the duad for each selected streamwise spacing, to the most extent at the shortest streamwise spacing, $h = 0.4$. Third, the efficiency for $\phi_2 = 180°$ is minimally dependent on $\phi_3$ and is usually higher than those for other $\phi_2$'s at a given $h$. This prediction can be explained by the argument that the efficiency of a foil duad for $\phi_2 = 180°$ is much higher than those for other $\phi_2$'s, (Fig. 12). Adding a trailing foil to the duad hardly overturns this advantage. Fourth, only for $\phi_2 = 180°$ is the foil-triad efficiency above the single-foil-propulsion level and independent of $\phi_3$. Notably, even the most efficient duad propulsion, $\phi_2 = 180°$, cannot compete with a single-foil propulsion. Moreover, for $\phi_2 = 180°$, the configurations with $\phi_3 = 0°$ (90°) and $\phi_3 = 180°$ (270°) are exactly the same, which is reflected in the computational findings (Fig. 12).

### 3.2.3 Weihs's Inviscid Versus the Present Viscous Computations

To compare with Weihs's inviscid analysis [27], the wake flow of a foil duad with $\phi_2 = 180°$ and $d = 0.4$ is analyzed. Figure 13 shows the periodic-mean horizontal velocity profiles at selected streamwise stations, from the trailing edge to two chord-length downstream further. Imaging a third foil existing midway ($y = 0$)



https://doi.org/10.1017/jmech.2011.21 Published online by Cambridge University Press

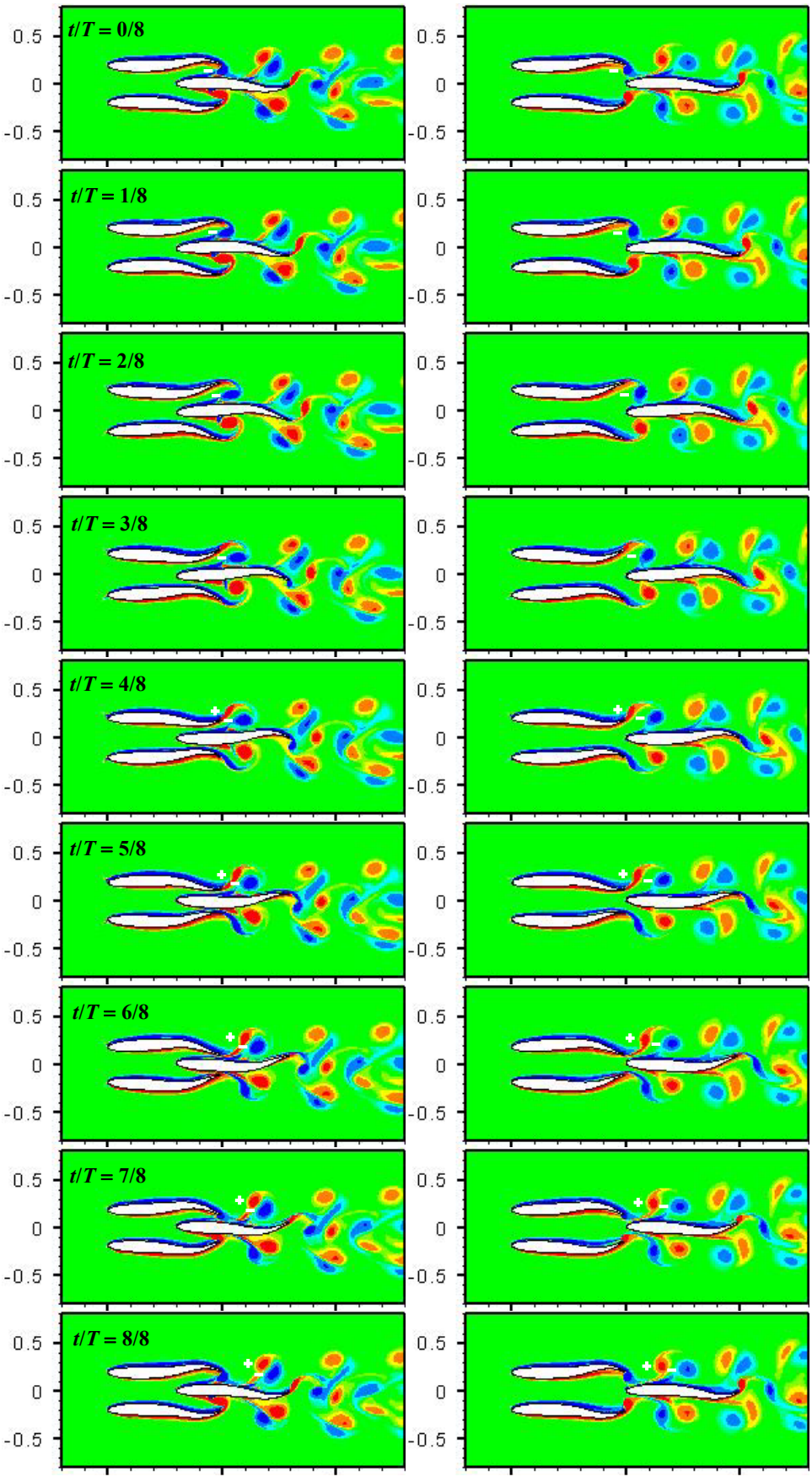



Fig. 11 Vorticity contour snapshot series taken in the sixth period of undulation for the foil triad with $\phi_2 = 180°$, $\phi_3 = 0°$, $d = 0.4$ and (a) $h = 0.6$ (b) $h = 1$. The positive and negative vortices shedding from Foil 1 are respectively marked plus and minus sign in white



https://doi.org/10.1017/jmech.2011.21 Published online by Cambridge University Press

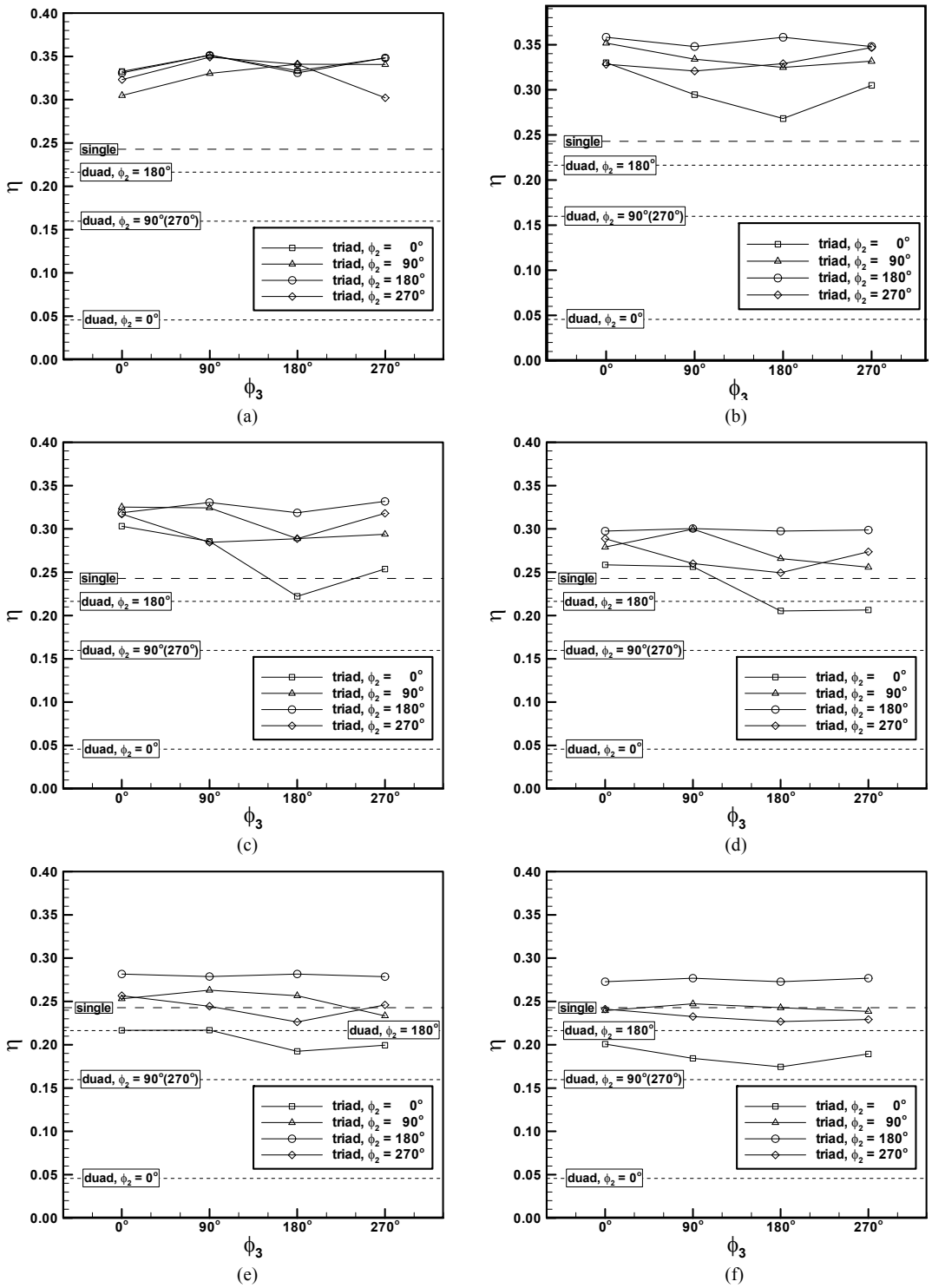



Fig. 12 Triad thrust efficiency as function of trailing-foil phase angle, $\phi_3$, at various phase differences between two leading foils, $\phi_2$, for $d$ = 0.4 and (a) $h$ = 0.6 (b) $h$ = 0.8 (c) $h$ = 0.9 (d) $h$ = 1 (e) $h$ = 1.1 (f) $h$ = 1.2. Also shown for comparison are the thrust efficiencies of the single-foil and the foil-duad propulsion

Table 1 Kinematics of the vortex pair shedding from Foil 1 at $t/T$ = 5/8 in Fig. 11

| $h$ | $\omega_+$ [a] | $\omega_-$ [a] | $R$ | $\alpha$ |
|---|---|---|---|---|
| 0.6 | 47.93 | –34.70 | 0.1593 | 50.53 |
| 1 | 43.79 | –26.54 | 0.2389 | 78.12 |

a: $\omega_+$ = maximal positive vorticity and $\omega_-$ = minimal negative vorticity in the vortex pair



https://doi.org/10.1017/jmech.2011.21 Published online by Cambridge University Press

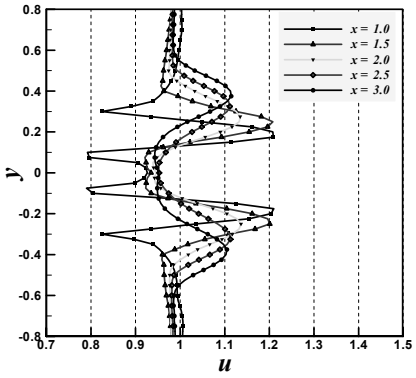



Fig. 13 Predicted periodic-mean horizontal velocity profiles at selected streamwise stations, from the leading edge ($x$ = 1) to three chord length further downstream ($x$ = 4) for the foil-duad propulsion with side-by-side arrangement separated by 0.4 chord length ($d$ = 0.4)

downstream of the duad, the flow velocity felt by this trailing foil is approximately 0.93 ~ 0.95 for $h$ increasing from 1 to 3 (Fig. 13). The drag of the trailing foil will be reduced by only 13.5% ~ 10% correspondingly, according to Weihs's argument that drag is proportional to flow velocity squared. For $d$ = 0.4, the two reverse Kármán vortex streets (one shed from each leading foil) are close enough to each other that a velocity deficit is generated on the wake centerline ($y$ = 0). For wider lateral separations, the two vortex streets would interact to a lesser extent, hence generating a weaker velocity deficit. In brief, for small $d$, the optimal position of the trailing foil should be in the near wake region of the leading foil; for large $d$, there would be no preferred position. However, according to the potential calculation of Weihs [27], the best position of the trailing foil is downstream of the trailing edges of the leading foils, > 5 times the distance between two vortices of the same sign in the vortex street of a leading foil, equivalent to $h$ > 4 based on the present simulation (Fig. 11). That is, the foils school in a diamond pattern. Taking this position, the drag of the trailing foil will decrease by 75% ~ 84% and the whole school will experience, on the average, 1/3 ~ 1/2 the drag experienced by a single propulsive foil. The significant contradiction in position and strength between the results of Weihs [27] and this work is mainly caused by the viscous effect which was not considered in the potential flow analysis. The viscous dissipation rapidly reduces the strength of vortices in the vortex wake, as illustrated by the fast decrease of velocity gradient from $x$ = 1 to $x$ = 3 (Fig. 13). Weihs assumed an infinite number of foils in the leading row and each leading foil shedding an infinite number of constant-strength trailing vortices, therefore the midway velocity always can be reduced for any lateral separation at sufficiently distant streamwise stations. However, the viscous effect greatly spoils the constant-strength assumption. Meanwhile, for a reference trailing foil, the nearest duad in the leading row will have much stronger influence than other foils in the same row if the viscous effect is considered. Hence, even for small $d$, significant vortex-to-vortex interaction is confined to the near wake region. Eventually, the amount of drag/velocity reduction turns to be much less than that predicted by Weihs's model.

To further demonstrate the difference in velocity reduction downstream of the anti-phase foil duad between the present and the Weihs's predictions [27], Fig. 14 shows the periodic-mean horizontal velocity at various stations on the wake centerline ($y$ = 0), as function of lateral distance between foils. The curve of Weihs [27] at the station $x$ = 4 is depicted assuming that the drag on a undulating foil within the school is three times that on a single stretched out foil and $b/a$ = 0.3, where $b$ and $a$ denote the distances between vortices with opposite and same sign respectively in the reverse Kármán vortex street. The ratio $b/a$ calculated in the present work is nearly constant (0.33) against the variation of $d$ and $x$, close to 0.3 used in the curve of Weihs [27]. Obviously, the velocity reduction decreases with increasing lateral distance in Weihs's analysis. However, it can be as much as 70% even for the widest separation studied ($d$ = 1). By contrast, in the present analysis, there exists very little velocity reduction at the three stations, $x$ = 1, 2, and 3, regardless of the lateral distance of foils. We note that, according to Weihs's model, the velocity reduction increases with $b/a$ and that in the viscous wake flow, the velocity reduction decreases with $x$. Therefore, the difference will be enlarged if the viscous data at $x$ = 4 is compared with the inviscid one with $b/a$ = 0.33.

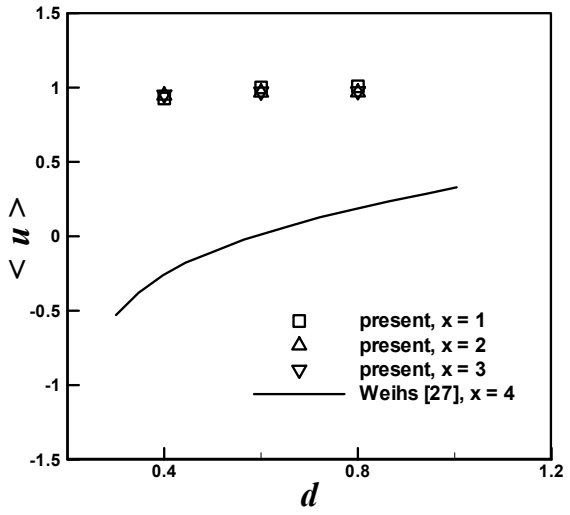



Fig. 14 Foil-duad periodic-mean streamwise velocity at various stations midway between the two foils and diagonally behind them, as function of lateral distance between foils. The data curve of Weihs [27] corresponds to that with $b/a$ = 0.3 and $T_1 = 3D_s$ in Fig. 4 of his work. $b$ and $a$ denote respectively the distances between vortices with opposite and same sign in the reverse Kármán vortex street. $T_1$ and $D_s$ denote respectively the drag on a swimming fish within the school and the drag on a single stretched out fish



https://doi.org/10.1017/jmech.2011.21 Published online by Cambridge University Press

For a foil triad, the viscous computations show that the trailing foil indeed has slightly better efficiency than a single propulsive foil if the triad configuration takes some particular "diamond" shapes, *i.e.* $h = 1.6$ and 2 for small lateral separations, $d = 0.4$ or $d = 0.5$. The maximal percentage increase of efficiency, roughly 32%, occurs for $d = 0.4$ and $h = 1.6$ (Fig. 6). These findings are qualitatively consistent with the reasoning from the viscous computational results of the foil duad. However, the efficiency of the foil triad increases by only about 10% at this combination of $d$ and $h$. In fact, according to the present viscous calculation, the optimal configuration is $d = 0.4$ and $h = 0.8$, which can generate a percentage increase of the triad efficiency as high as about 48%. Different from that suggested by Weihs, the mechanism behind is not directly related to the thrust vortices (reverse Kármán vortex streets), but to the interaction between the leading-foil undulation and the obstacle effect of the trailing foil as explained above.

## 4. CONCLUDING REMARKS

We have investigated hydrodynamics of foil triad with one foil following two to provide insight into flow characteristics of this novel thrust generator at intermediate Reynolds number. The hydrodynamic performance and unsteady flow structures were analyzed for various parameters, including the lateral spacing between the leading foils, the streamwise spacing between the leading and the trailing foils, and the relative phase difference of the undulating motion of each foil. The core of findings in the present work is given below.

To achieve highest efficiency (~36%) at $\phi_2 = 180°$, $d = 0.4$ and $h = 0.8$ is the best combination. The underlying mechanism is the leading-foil-shed vortices interacting with the boundary-layer vortices on the trailing-foil surface. This interaction produces a sufficiently small vortex-pair jet angle that the thrust-force increment can compensate for the increase of power consumption, that is, efficiency is raised. When the vortex pair is about to shed from the leading foil, a strong Venturi flow correspondingly appears in the gap region between the posterior part of the leading foil and the anterior part of the trailing foil. The predicted best position, $h = 0.8$, corresponds to the leading edge of the trailing foil being located 0.2 chord length upstream of the trailing edges of the leading foils. This current optimal triad formation is different from the diamond pattern derived by Weihs.

For $\phi_2 = 180°$, that is, the two leading foils perform anti-phase undulating motions, the thrust efficiency of the foil triad is higher than or equal to those for other $\phi_2$'s and varies little with $\phi_3$, *i.e.*, independent of the undulating motion of the trailing foil. Therefore, $\phi_2 = 180°$ should be a good choice because the trailing foil does not need to tune its undulating phase to a specific value.


## ACKNOWLEDGMENTS

We would like to thank the National Science Council of Taiwan R.O.C. for financially supporting this research under Contract No. NSC 96-2221-E-022-009-MY3. Ted Knoy is appreciated for his editorial assistance.


## REFERENCES


1. Wolfgang, M., Anderson, J. M., Grosenbaugh, M. A., Yue, D. K. P. and Triantafyllou, M. S., "Nearbody Flow Dynamics in Swimming Fish," *Journal of Experimental Biology,* **202**, pp. 2303–2327 (1999).
2. Barrett, D. S., Triantafyllou, M. S., Yue, D. K. P., Grosenbaugh MA, M. A. and Wolfgang, M., "Drag Reduction in Fish-Like Locomotion," *Journal of Fluid Mechanics,* **392**, pp. 183–212 (1999).
3. Stamhuis, E. and Videler, J., "Quantitative Flow Analysis Around Aquatic Animals Using Laser Sheet Particle Image Velocimetry," *Journal of Experimental Biology,* **198**, pp. 283–294 (1995).
4. Drucker, E. and Lauder, G., "Locomotor Forces on a Swimming Fish: Three Dimensional Vortex Wake Dynamics Quantified Using Digital Particle Image Velocimetry," *Journal of Experimental Biology,* **202**, pp. 2393–2412 (1999).
5. Wilga, C. D. and Lauder, G. V., "Hydrodynamic Function of the Shark's Tail," *Nature (London)*, **430**, pp. 850–850 (2004).
6. Triantafyllou, M. S., Triantafyllou, G. S. and Yue, D. K. P., "Hydrodynamics of Fishlike Swimming," *Annual Review of Fluid Mechanics*, **32**, pp. 33–53 (2000).
7. Lighthill, M. J., "Note on the Swimming of Slender Fish," *Journal of Fluid Mechanics,* **9**, pp. 305–317 (1960).
8. Wu, T. Y., "Swimming of a Waving Plate," *Journal of Fluid Mechanics,* **10**, pp. 321–344 (1961).
9. Chopra, M. G. and Kambe, T., "Hydromechanics of Lunate-Tail Swimming Propulsion," *Journal of Fluid Mechanics,* **79**, pp. 375–392 (1977).
10. Cheng, J. Y., Zhuang, L. X. and Tong, B. G., "Analysis of Swimming of Three-Dimensional Waving Plates," *Journal of Fluid Mechanics,* **232**, pp. 341–355 (1991).
11. Zhu, Q., Wolfgang, M. J., Yue, D. K. P. and Triantafyllou, M. S., "Three Dimensional Flow Structures and Vorticity Control in Fish-Like Swimming," *Journal of Fluid Mechanics,* **468**, pp. 1–28 (2002).
12. Fauci, L. J., "A Computational Model of the Fluid Dynamics of Undulatory and Flagellar Swimming," *American Zoologist,* **36**, pp. 599–607 (1996).
13. Liu, H., Wassenberg, R. and Kawachi, K., "A Computational Fluid Dynamics Study of Tadpole Swimming," *Journal of Experimental Biology,* **199**, pp. 1245–1260 (1996).
14. Liu, H., Wassenberg, R. and Kawachi, K., "The Three-Dimensional Hydrodynamics of Tadpole




https://doi.org/10.1017/jmech.2011.21 Published online by Cambridge University Press

Swimming," *Journal of Experimental Biology,* **200**, pp. 2807–2819 (1997).
15. Carling, J., Williams, T. L. and Bowtell, G., "Self-Propelled Anguilliform Swimming: Simultaneous Solution of the Two-Dimensional Navier-Stokes Equations and Newton's Laws of Motion," *Journal of Experimental Biology,* **201**, pp. 3143–3166 (1998).
16. Shen, L., Zhang, X., Yue, D. K. P. and Triantafyllou, M. S., "Turbulent Flow Over a Flexible Wall Undergoing a Streamwise Travelling Wave Motion," *Journal of Fluid Mechanics,* **484**, pp. 197–221 (2003).
17. Dong, G. J. and Lu, X. Y., "Numerical Analysis on the Propulsive Performance and Vortex Shedding of Fish-Like Travelling Wavy Plate," *International Journal for Numerical Methods in Fluids,* **48**, pp. 1351–1373 (2005).
18. Wu, J. Z., Pan, Z. L. and Lu, X. Y., "Unsteady Fluid-Dynamic Force Solely in Terms of Control-Surface Integral," *Physics of Fluids,* **17**, 098102 (2005).
19. Liao, J. C., Beal, D. N., Lauder, G. V. and Triantafyllou, M. S., "The Kármán Gait: Novel Body Kinematics of Rainbow Trout Swimming in a Vortex Street," *Journal of Experimental Biology,* **206**, pp. 1059–1073 (2003).
20. Liao, J. C., Beal, D. N., Lauder, G. V. and Triantafyllou, M. S., "Fish Exploiting Vortices Decrease Muscle Activity," *Science*, **302**, pp. 1566–1569 (2003).
21. Beal, D. N., Hower, F. S., Triantafyllou, M. S., Liao, J. C. and Lauder, G. V., "Passive Propulsion in Vortex Wakes," *Journal of Fluid Mechanics,* **549**, pp. 385–402 (2006).
22. Gopalkrishnan, R., Triantafyllou, M. S., Triantafyllou, G. S. and Barrett, D., "Active Vorticity Control in a Shear Flow Using a Flapping Foil," *Journal of Fluid Mechanics,* **274**, pp. 1–21 (1994).
23. Streitlien, K., Triantafyllou, G. S. and Triantafyllou, M. S., "Efficient Foil Propulsion Through Vortex Control," *American Institute of Aeronautics and Astronautics,* **34**, pp. 2315–2319 (1996).
24. Parrish, J. K. and Keshet, L. E., "Complexity, Pattern and Evolutionary Trade-Offs in Animal Aggregation," *Science*, **284**, pp. 99–101 (1999).
25. Stöker, S., "Models for Tuna School Formation," *Mathematical Bioscience,* **156**, pp. 167–190 (1999).
26. Weihs, D., "Hydromechanics of Fish Schooling," *Nature (London)*, **241**, pp. 290–291 (1973).
27. Weihs, D., "Some Hydrodynamical Aspects of Fish Schooling," *Swimming Flying Nature*, **2**, pp. 703–718 (1975).
28. Partridge, B. L. and Pitcher, T. J., "Evidence Against a Hydrodynamic Function for Fish Schools," *Nature (London)*, **279**, pp. 418–419 (1979).
29. Keenleyside, M. H. A., "Some Aspects of the Schooling Behaviour of Fish," *Behaviour,* **8**, pp. 183–247 (1955).
30. Jian, D., Shao, X.-M. and Ren, A.-L., "Numerical Study on Propulsive Performance of Fish-Like Swimming Foils," *Journal of Hydrodynamics*, **18**, pp. 681–687 (2006).
31. Dong, G. J. and Lu, X. Y., "Characteristics of Flow Over Traveling-Wavy Foils in a Side-By-Side Arrangement," *Physics of Fluids,* **19**, 057107 (2007).
32. Kelly, S. D. and Xiong, H. L., "Controlled Hydrodynamic Interactions in Schooling Aquatic Locomotion," *Proceedings of the 44th IEEE Conference on Decision and Control*, *and the European Control Conference 2005,* Seville, Spain, December 12-15, pp. 3904–3910 (2005).
33. Eldredge, J., Hector, D. and Kelly, S., "Computations of Wake Dynamics in a Simple Model for Fish Schooling," *SIAM Conference on Applications of Dynamical Systems*, Snowbird, Utah (2007).
34. Breder, C. M., "Fish Schools as Operational Structures," *Fishery Bulletin of the Fish and Wildlife Service*, **74**, pp. 471–502 (1976).
35. Chung, M-H., "On Burst-And-Coast Swimming Performance in Fish-Like Locomotion," *Bioinspiration and Biomimetics,* **4**, 036001 (2009).
36. Chung, M-H., "Cartesian Cut Cell Approach for Simulating Incompressible Flows with Rigid Bodies of Arbitrary Shape," *Computers and Fluids*, **35**, pp. 607–623 (2006).
37. Chung, M-H., "Numerical Study of Rowing Hydrofoil Performance at Low Reynolds Numbers," *Journal of Fluids and Structures*, **24**, pp. 313–335 (2008).
38. Bohl, D. G. and Koochesfahani, M. M., "MTV Measurements of the Vortical Field in the Wake of an Airfoil Oscillating at High Reduced Frequency," *Journal of Fluid Mechanics*, **620**, pp. 63–88 (2009).
39. Milne-Thompson, L. M., "*Theoretical Aerodynamics*," Macmillan, New York (1966).

(Manuscript received November 3, 2009,
accepted for publication July 4, 2010.)



https://doi.org/10.1017/jmech.2011.21 Published online by Cambridge University Press